# Supporting Information

## Tuning the Solvation Environment of Polyoxometalate Redox-Active Species to Boost Thermo-Electrochemical Cell Performance

Shunsuke Okata,[†,a] Katsuhiro Wakamatsu,[†,*,a,b] Riku Hosokawa,[a] Kazuma Iwata,[b] Kohei Tada,[c] and Hirofumi Yoshikawa*[,a,b]

[a] Department of Nanotechnology for Sustainable Energy, Graduate School of Science and Technology, Kwansei Gakuin University, 1 Gakuen Uegahara, Sanda, Hyogo 669-1330, Japan

[b] Program of Materials Science, School of Engineering, Kwansei Gakuin University, 1 Gakuen Uegahara, Sanda, Hyogo 669-1330, Japan

[c] Department of Marerials Engineering Science, Graduate School of Engineering Science, Osaka University, 1-3 Machikaneyama, Toyonaka, Osaka 560-8531, Japan

† K.W. and S.O. contributed equally to this work and share first authorship.

* Corresponding authors. Email addresses: katsu29yukke@gmail.com (K.W.)
yoshikawah@kwansei.ac.jp (H.Y.)

## Structural and redox stability of POM in DMSO-containing electrolytes

To gain deeper insight into the effect of DMSO on POM behaviour, CV, FT-IR spectroscopy, and PXRD were employed to evaluate structural and electronic changes. As shown in Figure S2(a), both acetonitrile (MeCN) and MeCN:DMSO systems exhibit similar redox peak profiles, indicating that the intrinsic redox behaviour of POM is not significantly affected by DMSO addition. This observation implies that $S_e$ enhancement does not originate from changes in the electronic (inner-sphere) structure of POM but rather from entropy variations in the outer-sphere solvation environment.

The FT-IR and XRD results (Figure S2(b) and S2(c)) further confirmed that no significant changes occur in the crystal structure or major chemical bonds of POM after DMSO addition. Combined with the electrochemical data, these findings corroborate that the enhancement in $S_e$ arises primarily from modifications to the solvation structure rather than from structural alteration of the POM framework itself.

## Supplementary figures

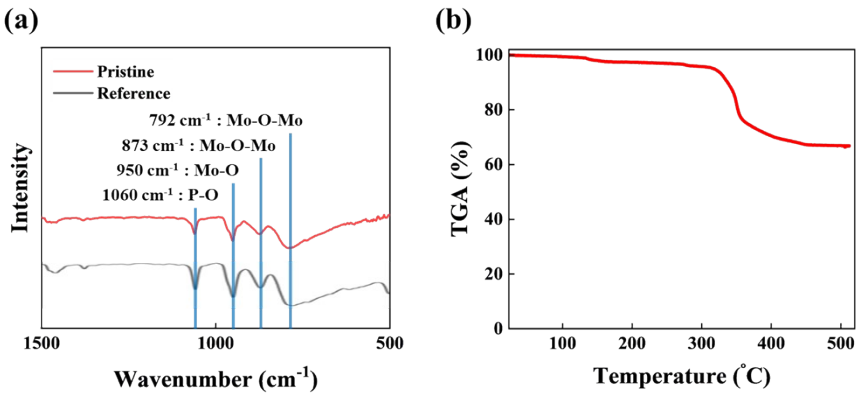


**Figure S1.** (a) FT-IR spectrum and (b) TG curve of Keggin-type POM ($TBA_3[PMo_{12}O_{40}]$). Simulated profiles for $TBA_3[PMo_{12}O_{40}]$ powder are taken from Ref. [1,2].

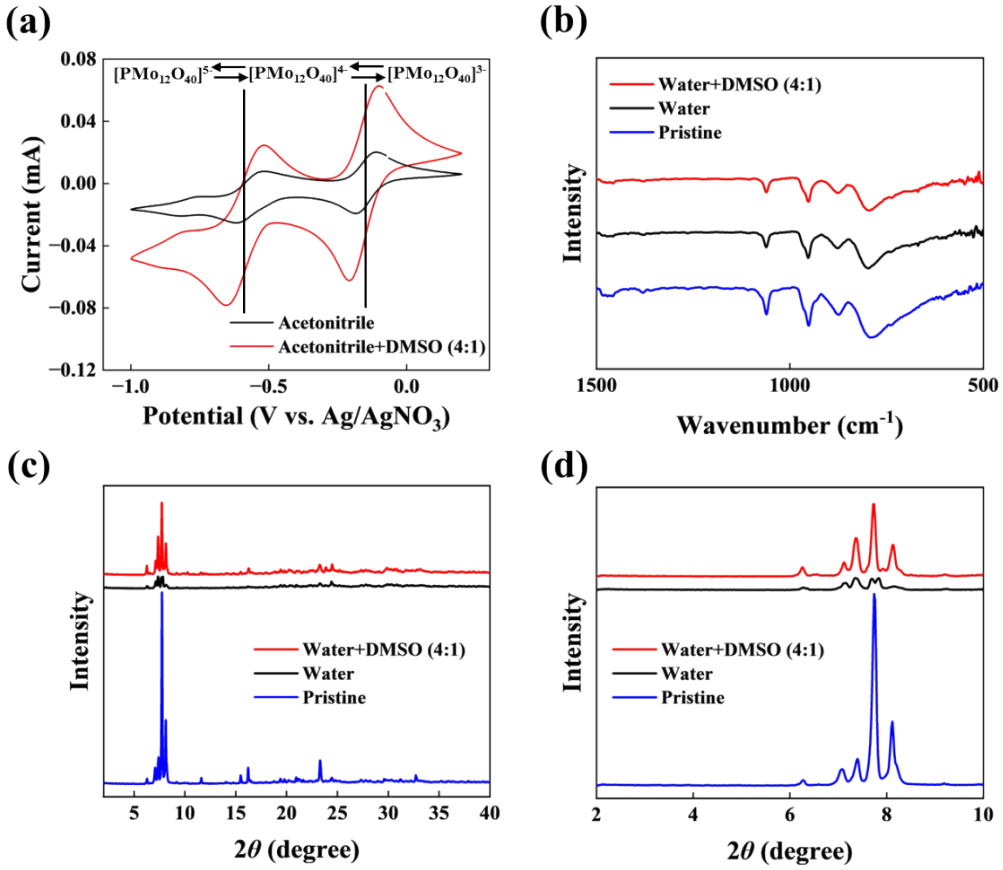


**Figure S2.** (a) CV curve of Keggin-type POM ($TBA_3[PMo_{12}O_{40}]$) in MeCN and MeCN:DMSO = 4:1 mixed solutions. $[PMo_{12}O_{40}]^{5-} \rightleftarrows [PMo_{12}O_{40}]^{4-} \rightleftarrows [PMo_{12}O_{40}]^{3-}$ redox reaction reported in the Ref. [3]. (b) FT-IR spectra and (c) PXRD patterns of the dried POM samples, and (d) an enlarged view (a $2\vartheta$ range of 2–10°).

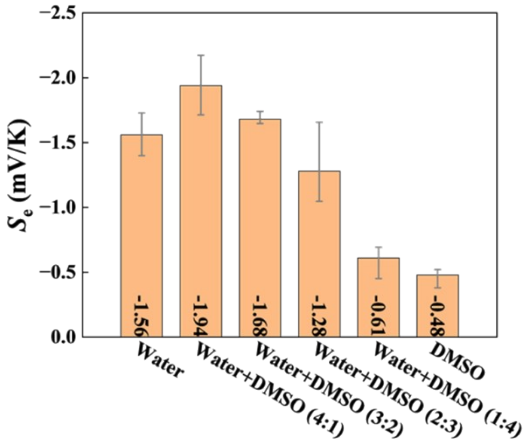


**Figure S3.** Comparison of the Seebeck coefficient values based on solvent composition in water/DMSO mixed electrolytes containing Keggin-type POM ($TBA_3[PMo_{12}O_{40}]$). The legend follows the same conventions as in Figure 2.

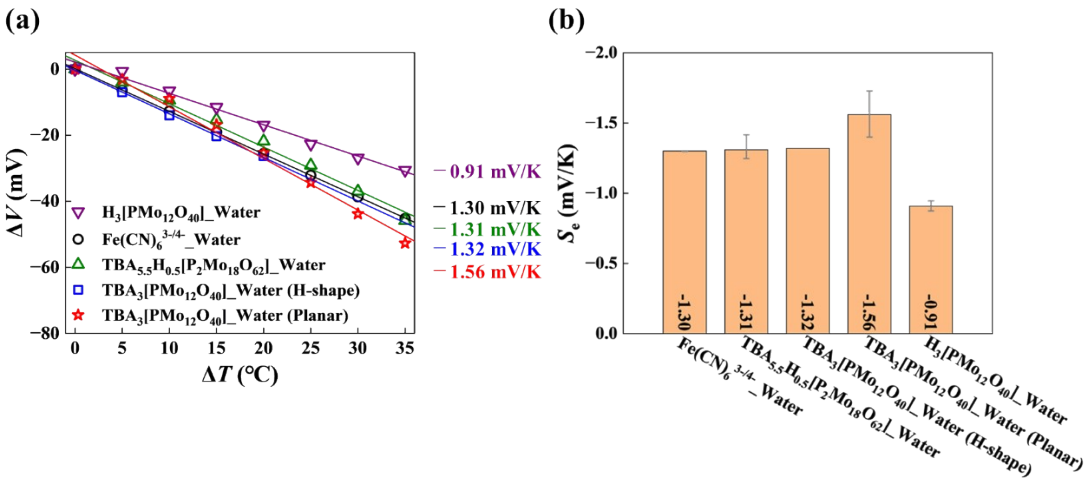


**Figure S4.** (a) Dependence of the Seebeck coefficient and (b) Comparison of the Seebeck coefficient values based on solvent composition in water electrolytes containing $Fe(CN)_6^{3-/4-}$, Wells-Dawson-type POM ($TBA_{5.5}H_{0.5}[P_2Mo_{18}O_{62}]$) and Keggin-type POMs ($TBA_3[PMo_{12}O_{40}]$ and $H_3[PMo_{12}O_{40}]$).

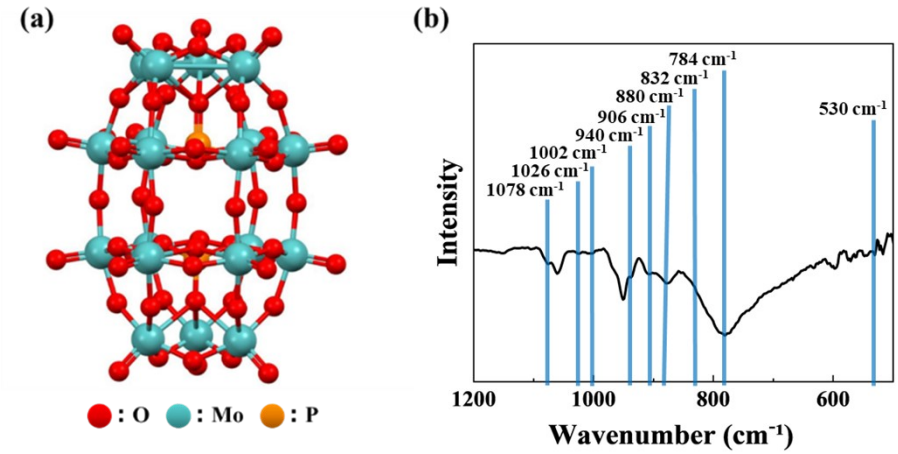


**Figure S5.** (a) Structure of the Wells-Dawson-type POM anion ($[P_2Mo_{16}O_{62}]^{6-}$) and (b) IR spectrum of the synthesized $TBA_{5.5}H_{0.5}[P_2Mo_{18}O_{62}]$. Peaks at 1078, 1026, 1002, 940, 906, 880, 832, 784, and 530 $cm^{-1}$ correspond to those reported in the Ref. [4].

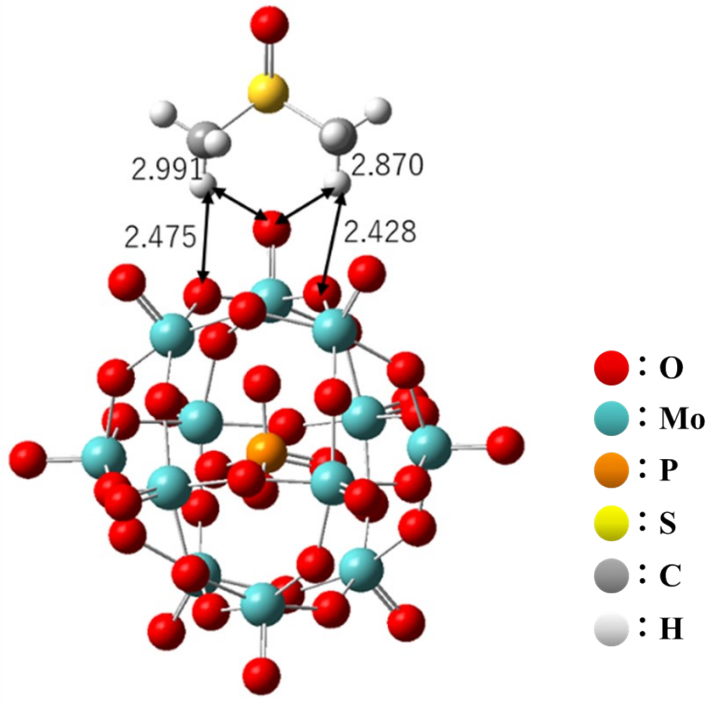


**Figure S6.** Converged structures of Keggin-type POM anion ($[PMo_{12}O_{40}]^{3-}$) and DMSO molecules obtained using DFT calculations. The numbers in the figure indicate intermolecular distances (Å).

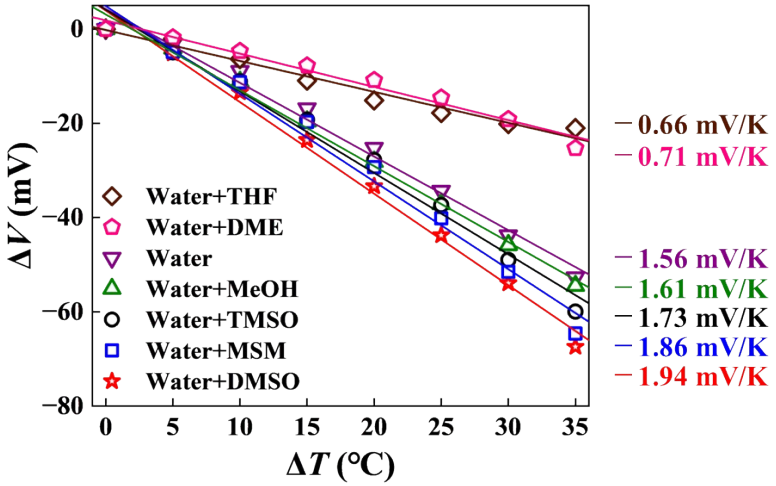


**Figure S7.** Dependence of the Seebeck coefficient on Keggin-type POM ($TBA_3[PMo_{12}O_{40}]$)-based electrolytes in different water/organic solvent systems at a fixed water-to-solvent volume ratio of 4:1 (20 vol%). MSM system prepared as a 3 M mixed solution because MSM is solid at room temperature (approximately 25 °C).

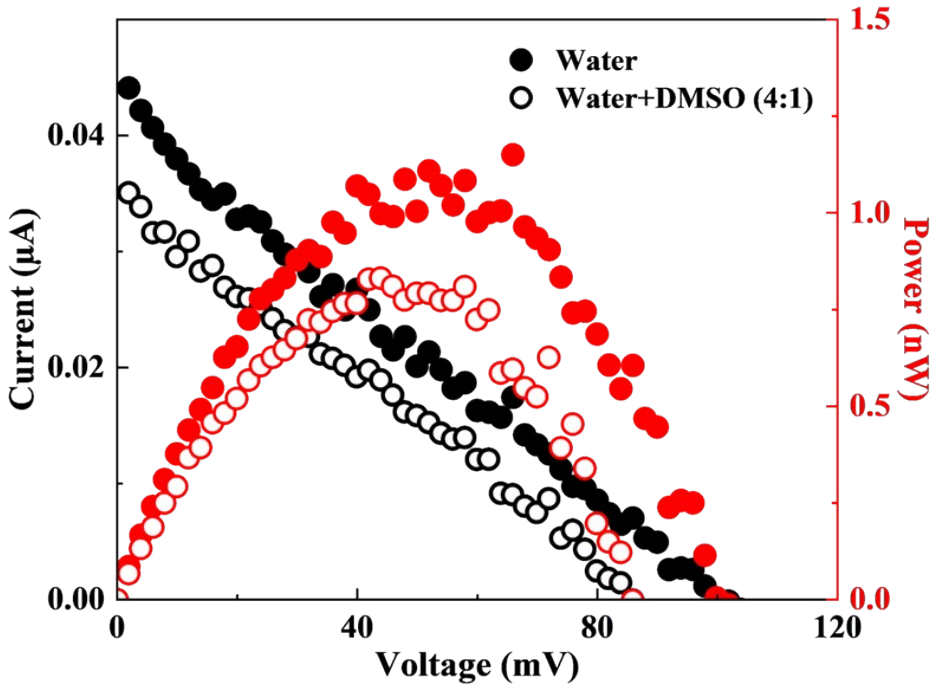


**Figure S8.** (a) LSV profiles and (b) calculated $P_{max}$ values of Keggin-type POM ($TBA_3[PMo_{12}O_{40}]$) in aqueous and water:DMSO = 4:1 mixed solutions.

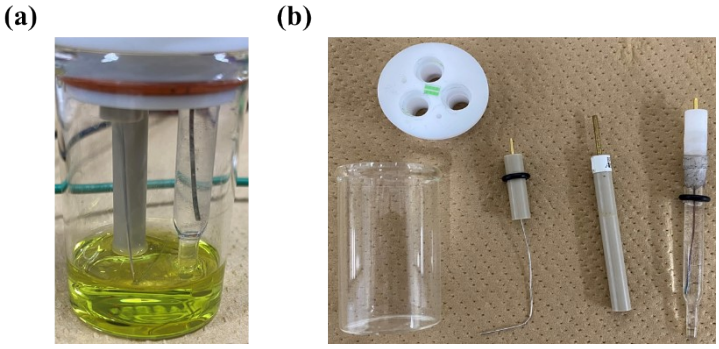


**Figure S9.** Configuration of the three-electrode voltammetry cell assembled with glassy carbon working, platinum wire counter electrode, and $Ag/AgNO_3$ reference electrodes for CV and EIS measurements: (a) cell after assembly and (b) individual components prior to assembly.

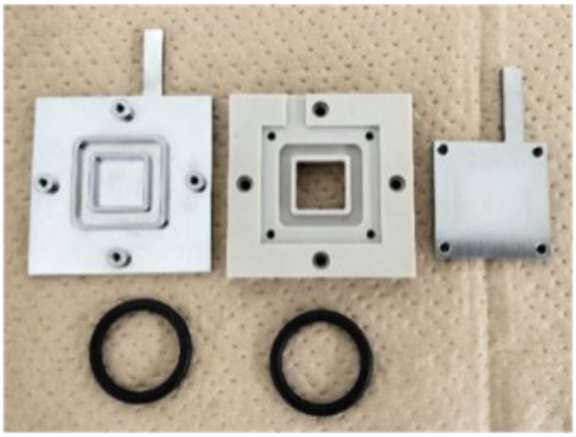

**Figure S10.** Configuration of the planar cell assembled with stainless steel electrodes, PEEK spacers, and O-rings for thermoelectric voltage and LSV measurements.

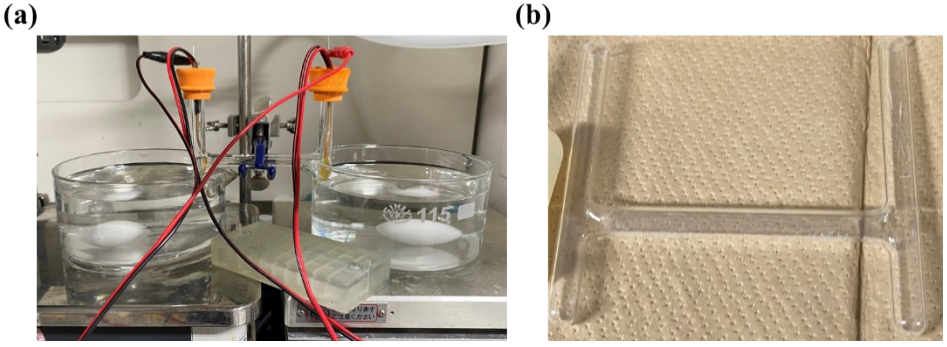


**Figure S11.** Configuration of the H-shape glass tube cell assembled with platinum wire electrodes and thin-film thermistors for thermoelectric voltage measurements: (a) cell

after assembly and (b) H-shape glass tube.

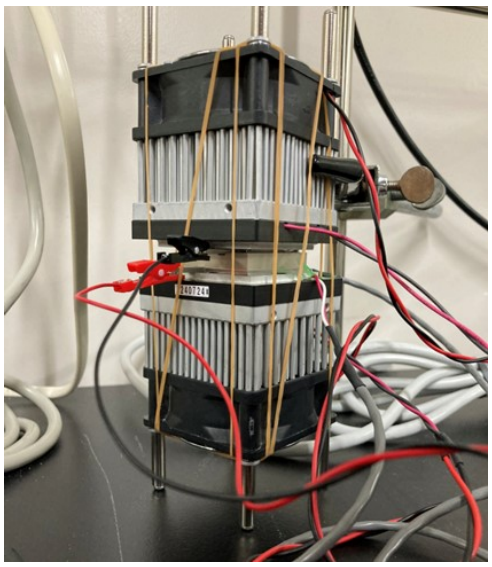

**Figure S12.** Configuration of the instrument setup assembled with a planar cell and Peltier temperature controller set for thermoelectric voltage and LSV measurements.

## Supplementary tables

**Table S1.** Seebeck coefficients measured using a planar cell for $Fe(CN)_6^{3-/4-}$, Wells-Dawson-type POM ($TBA_{5.5}H_{0.5}[P_2Mo_{18}O_{62}]$) and Keggin-type POMs ($TBA_3[PMo_{12}O_{40}]$ and $H_3[PMo_{12}O_{40}]$) as redox species. In A_B, A and B denote the solute and solvent, respectively, with the notation for B following that in Figure 2. Each value represents the average of 5-6 measurements, with the corresponding minimum and maximum values also indicated.

| Solvent | $S_e$ [mV/K] |
|---|---|
| $Fe(CN)_6^{3-/4-}$_Water | -1.30 (max: -1.30, min: -1.29) |
| $TBA_{5.5}H_{0.5}[P_2Mo_{18}O_{62}]$_Water | -1.31 (max: -1.42, min: -1.25) |
| $H_3[PMo_{12}O_{40}]$_Water | -0.91 (max: -0.94, min: -0.87) |
| $TBA_3[PMo_{12}O_{40}]$_Water | -1.56 (max: -1.73, min: -1.40) |
| $TBA_3[PMo_{12}O_{40}]$_Water+DMSO (4:1) | -1.94 (max: -2.18, min: -1.72) |
| $TBA_3[PMo_{12}O_{40}]$_Water+DMSO (3:2) | -1.68 (max: -1.74, min: -1.65) |
| $TBA_3[PMo_{12}O_{40}]$_Water+DMSO (2:3) | -1.28 (max: -1.66, min: -1.05) |
| $TBA_3[PMo_{12}O_{40}]$_Water+DMSO (1:4) | -0.61 (max: -0.69, min: -0.45) |
| $TBA_3[PMo_{12}O_{40}]$_DMSO | -0.48 (max: -0.52, min: -0.38) |
| $TBA_3[PMo_{12}O_{40}]$_Water+MeOH (4:1) | -1.61 (max: -1.73, min: -1.45) |
| $TBA_3[PMo_{12}O_{40}]$_Water+THF (4:1) | -0.66 (max: -0.73, min: -0.51) |
| $TBA_3[PMo_{12}O_{40}]$_Water+DME (4:1) | -0.71 (max: -1.02, min: -0.37) |
| $TBA_3[PMo_{12}O_{40}]$_Water+TMSO (4:1) | -1.73 (max: -2.31, min: -1.19) |
| $TBA_3[PMo_{12}O_{40}]$_Water+MSM (3 M) | -1.86 (max: -2.02, min: -1.74) |

**Table S2.** Dielectric constants, molecular dipole moments, and viscosities of water and representative organic additives used in this study. Note that 1 D = $3.33564 \times 10^{-30}$ C · m and 1 cP = 1 mPa · s.

| Solvent | Dielectric constant | Molecular dipole moment [D] | Viscosity [cP] | Reference |
|---|---|---|---|---|
| Water | 80 | 2.9 | 1.002 (20 °C) | [5,6] |
| MeOH | 32.7 | 1.7 | 0.541 (25 °C) | [7,8] |
| THF | 7.6 | 1.75 | 0.555 (20 °C) | [7,9] |
| DME | 7.3 | 1.71 | 0.455 (25 °C) | [10,11] |
| TMSO | 42.8 | 4 | 9.87 (30 °C) | [12,13] |
| MSM | 47.39 | 4.44 | — | [14,15] |
| DMSO | 46.6 | 3.9 | 2 (20 °C) | [7,9] |

**Table S3.** Performance metrics of representative redox-active molecules as thermoelectric materials for TECs reported in this study and in previous work. Parameters include $S_e$: Seebeck coefficient and $P_{max}$: maximum power output values.

| Redox species | Solvent | Additive | Temperature | $S_e$ [mV/K] | $P_{max}$ | Reference |
|---|---|---|---|---|---|---|
| $PMo_{12}O_{40}$ | Water | — | 25~60 °C | 1.56 | 1.150 nW (30 K) | This work |
| $PMo_{12}O_{40}$ | Water | DMSO | 25~60 °C | 1.94 | 0.831 nW (30 K) | This work |
| $Fe(CN)_6^{3-/4-}$ | Water | — | $\Delta T$ = 30 K (25~55 °C) | 1.43 | — | [16] |
| $Fe(CN)_6^{3-/4-}$ | Water | Hexan | | 1.43 | — | |
| $Fe(CN)_6^{3-/4-}$ | Water | EtOH | | 2.9 | — | |
| $Fe(CN)_6^{3-/4-}$ | Water | MeOH | | 2.9 | 58 μW/K²m | |
| $Fe(CN)_6^{3-/4-}$ | Water | DMSO | | 2.9 | — | |
| $Fe(ClO_4)_{2/3}(Fe^{2+/3+})$ | Water | — | $\Delta T$ = 20 K (25~45 °C) | 1.48 | 35 nW (10 K) | [17] |
| $Fe(ClO_4)_{2/3}(Fe^{2+/3+})$ | Water | MeOH | | 1.47 | — | |
| $Fe(ClO_4)_{2/3}(Fe^{2+/3+})$ | Water | Acetone | | 1.57 | — | |
| $Fe(ClO_4)_{2/3}(Fe^{2+/3+})$ | Water | TMS | | 2.09 | 50 nW (10 K) | |
| $Fe(ClO_4)_{2/3}(Fe^{2+/3+})$ | Water | DMSO | | 0.78 | 16 nW (10 K) | |
| $Co(bpy)_3(NTf_2)_{2/3}(Co^{2+/3+})$ | MPN | — | 20~140 °C | 2.19 | 499 mW/m² (10 K) | [18] |
| $Co(bpy)_3(NTf_2)_{2/3}(Co^{2+/3+})$ | $[C_2mim][eFAP]$ | — | | 1.88 | 22 mW/m² (10 K) | |
| $Co(bpy)_3(NTf_2)_{2/3}(Co^{2+/3+})$ | $[C_2mim][NTf_2]$ | — | | 1.64 | 133 mW/m² (10 K) | |
| $Co(bpy)_3(NTf_2)_{2/3}(Co^{2+/3+})$ | $[C_2mim][B(CN)_4]$ | — | | 1.55 | 165 mW/m² (10 K) | |
| $Co(bpy)_3(NTf_2)_{2/3}(Co^{2+/3+})$ | $[C_4mpyr][NTf_2]$ | — | | 1.56 | — | |
| $Co(bpy)_3(NTf_2)_{2/3}(Co^{2+/3+})$ | $[C_4mim][BF_4]$ | — | | 1.40 | — | |
| $I_3^-/I^-$ | Water | — | $\Delta T$ = 34 K (10~44 °C) | 0.86 | — | [19] |
| $I_3^-/I^-$ | Water | α-CD | | 1.45 | — | |
| $I_3^-/I^-$ | Water | α-CD, KCl | | 1.97 | — | |
| $[PW_{12}O_{40}]^{3-/4-}$ | Water | — | 19~55 °C | 0.5 | — | [20] |
| $[PW_{12}O_{40}]^{4-/5-}$ | Water | — | | 0.91 | — | |
| $[PW_{12}O_{40}]^{5-/6-}$ | Water | — | | 1.1 | — | |
| $[VW_{12}O_{40}]^{3-/4-}$ | Water | — | | 0.6 | — | |
| $[VW_{12}O_{40}]^{4-/5-}$ | Water | — | | 0.88 | — | |
| $[VW_{12}O_{40}]^{5-/6-}$ | Water | — | | 1.1 | — | |
| $[PVW_{11}O_{40}]^{4-/5-}$ | Water | — | | 0.84 | — | |
| $[PVW_{11}O_{40}]^{5-/6-}$ | Water | — | | 1.1 | — | |
| $[VVW_{11}O_{40}]^{4-/5-}$ | Water | — | | 0.69 | — | |
| $[VVW_{11}O_{40}]^{5-/6-}$ | Water | — | | 1.04 | — | |
| $[P_2W_{18}O_{62}]^{6-/12-}$ | Water | — | 5~50 °C | 1.7 | — | [21] |

## References


1 M. Pascual-Borràs, E. Arca, H. Yoshikawa, T. Penfold, P. G. Waddell and R. J. Errington, *J. Am. Chem. Soc.*, 2024, **146**, 26485–26496.

2 C. Rocchiccioli-Deltcheff, M. Fournier, R. Franck and R. Thouvenot, *Inorg. Chem.*, 1983, **22**, 207–216.

3 J. J. J. Chen and M. A. Barteau, *Journal of Energy Storage*, 2017, **13**, 255-261.

4 A S. Himeno, M. Hashimoto and T. Ueda, *Inorganica Chimica Acta*, 1999, **284**, 237-245.

5 Y. S. Badyal, M.-L. Saboungi, D. L. Price, S. D. Shastri, D. R. Haeffner and A. K. Soper, *J. Chem. Phys.*, 2000, **112**, 9206–9208.

6 L. Korson, W. Drost-Hansen and F. J. Millero, *J. Phys. Chem.*, 1969, **73**, 34–39.

7 S. Wu, Y. Luo, S. Niu, W. Lin and C. Fang, *J. Phys. Chem. Lett.*, 2025, **16**, 12010–12017.

8 S. Z. Mikhail and W. R. Kimel, *J. Chem. Eng. Data*, 1961, **6**, 533–537.

9 T. Prem Kumar, P. V. S. S. Prabhu, A. K. Srivastava, U. Bejoy Kumar, R. Ranganathan and R. Gangadharan, *J. Power Sources*, 1994, **50**, 283–294.

10 V. Viti and P. Zampetti, *Chemical Physics*, 1973, **2**, 233-238.

11 M. Yoshio, H. Nakamura, M. Hyakutake, S. Nishikawa and K. Yoshizuka, *Journal of Power Sources*, 1993, **41**, 77-86.

12 C. Laurence, P. Nicolet, M. T. Dalati, J. L. M. Abboud and R. Notario, *J. Phys. Chem.*, 1994, **98**, 5807–5816.

13 A. Fratiello and R. E. Schuster, *Inorg. Chem.*, 1969, **8**, 480–484.

14 T. Clark, J. S. Murray, P. Lane and P. Politzer, *J. Mol. Model.*, 2008, **14**, 689–697.

15 R. L. Burwell and C. H. Langford, *J. Am. Chem. Soc.*, 1959, **81**, 3799–3800.

16 T. Kim, J. S. Lee, G. Lee, H. Yoon, J. Yoon, T. J. Kang and Y. H. Kim, *Nano Energy*, 2017, **31**, 160–167.

17 Y. Liu, Q. Zhang, G. O. Odunmbaku, Y. He, Y. Zheng, S. Chen, Y. Zhou, J. Li, M. Li and K. Sun, *J. Mater. Chem. A*, 2022, **10**, 19690–19698.

18 T. J. Abraham, D. R. MacFarlane and J. M. Pringle, *Energy Environ. Sci.*, 2013, **6**, 2639–2645.

19 H. Zhou, T. Yamada and N. Kimizuka, *J. Am. Chem. Soc.*, 2016, **138**, 10502–10507.

20 M. Dagar, A. De, Z. Lu, E. M. Matson and A. E. Thorarinsdottir, *ACS Mater. Au*, 2025, **5**, 200–210.

21 E. S. Grape, J. Huang, D. Roychowdhury, T. T. Debela, H. Chang, A. Jenkins, A. M. Schimpf, C. H. Hendon and C. K. Brozek, *ACS Appl. Energy Mater*., 2024, **7**, 11423–11428.